ARTICLE

Scanning Photoelectrochemical Microscopic Study in Photoinduced Electron Transfer of Supramolecular Sensitizers-TiO_2 Thin Films Systems

Sheng-Ya Zhang, Min Yao, Ze Wang, Tian-Jiao Liu, Rong-Fang Zhang, Hui-Qin Ye, Yan-Jun Feng, Xiao-Quan Lu*

Key Laboratory of Bioelectrochemistry & Environmental Analysis of Gansu Province, College of Chemistry & Chemical Engineering, Northwest Normal University, Lanzhou, 730070, PR China

Abstract

Crafting charge transfer channels at titanium dioxide (TiO_2) based photoanodes remain a pressing bottleneck in solar-to-chemical conversion technology. Despite the tremendous attempts, TiO_2 as the promising photoanode material still suffers from sluggish charge transport kinetics. Herein, we propose an assembly strategy that involves the axial coordination grafting metalloporphyrin-based photosensitizer molecules (MP) onto the surface-modified TiO_2 nanorods (NRs) photoanode, forming the composite MP/TiO_2 NRs photoelectrode. As expected, the resulted unique MP_B/TiO_2 NRs photoelectrode displays significantly improved photocurrent density as compared to TiO_2 NRs alone and MP_A/TiO_2 NRs photoelectrode. Scanning photoelectrochemical microscopy (SPECM) and intensity modulated photocurrent spectroscopy (IMPS) were employed to systematically evaluate the continuous photoinduced electron transfer (PET) dynamics for MP/TiO_2 NRs photoelectrode. According to the data fitting, it is found that the photoelectron transfer rate (k_{eff}) constant for the MP_B/TiO_2 NRs is about 2.6 times higher than that for the pure TiO_2 NRs under light irradiation. The high kinetic constant for the MP_B/TiO_2 NRs was ascribed to that the conjugated molecules MP_B of D-A structure can effectively accelerate intramolecular electrons transfer as well as promote electrons taking part in the reduction reaction of I_3^- to I^- in the novel charge transfer channel. The results demonstrated in this study are expected to shed some light on investigating the mechanism in the charge transfer process of artificial photosynthesis and constructing efficient photoelectrodes.

Keywords: Photosensitizer; TiO_2 nanorods; Scanning photoelectrochemical microscopy; Photoexcited electron transfer

1. Introduction

The rapid development of global industry and the high energy demand have generated severe environmental concerns such as water contamination, air pollution, and greenhouse gas emissions [1−3]. Therefore, there is an increasing demand for ecofriendly and sustainable energy sources to replace fossil fuels. In recent years, solar energy with global distribution has been widely used as a clean and renewable energy source in terms of energy demand and environmental issues [4]. Photoelectrochemical (PEC) water splitting and photovoltaic power generation have attracted considerable attention as renewable energy sources through the direct conversion of solar energy [5−7]. However, the slow transfer rate of photoexcited carriers is extremely limited in practical applications to solve the energy crisis [8,9].

Photoelectrode is the key core part in the PEC water splitting system. In 1972, titanium dioxide (TiO_2) films as the photoanode for PEC water splitting was first demonstrated by Honda and Fujishima [10]. At the present stage, TiO_2 is the most researched and used semiconductor photoanode due to its outstanding chemical stability

Received 10 December 2022; Received in revised form 28 December 2022; Accepted 13 April 2023
Available online 23 April 2023

* Corresponding author, Xiao-Quan Lu, Tel: (86-931)7971276, E-mail address: luxq@nwnu.edu.cn.

https://doi.org/10.13208/j.electrochem.2218005

[11,12]. However, the inherent weaknesses of TiO_2, such as low carrier mobility, large bandgap and only responding to the ultraviolet light, have greatly hindered the TiO_2 practical application [13−15]. Following that, numerous research efforts have been made to realize a high solar conversion efficiency of TiO_2 [16−18]. Light absorption efficiency, carrier separation and transfer rates, and surface dynamics combine to influence photoanode PEC performance [19−21]. Among them, the photoinduced electron transfer (PET) rate is key to the efficient conversion of solar energy to chemical energy [20,22,23].

In typical dye-sensitized solar cells (DSSCs), nanocrystalline semiconductors (TiO_2, SnO_2, ZnO, etc.) decorated with photosensitizer molecules inject electrons upon photoexcitation into the conduction band of the semiconductor, achieving light energy conversion [24−26]. Sensitizers are an important component of DSSCs and they essentially determine the performance of DSSCs in terms of light harvesting and energy conversion [27]. Enlightened by these research progresses, we have attempted to assemble sensitizers molecules onto the surface of TiO_2 films to improve light absorption efficiency and facilitate electron transfer. Efficient sensitizer molecules should have the advantage of high light-harvesting capabilities in the visible to near-infrared region, allowing effective electron injection as well as inhibiting charge recombination [28,29]. To fulfill these requirements, numerous attempts have been made to develop organic dyes with a D-π-A structural motif, in which an electron donor (D) and an electron acceptor (A) are linked via a π-conjugated system [30−32]. To date, porphyrin sensitizers with a donor-(π bridge)-acceptor (D-π-A) structure have been used in DSSCs, showing the promising performance and the efficiencies which rival the best Ru(II) polypyridal dyes in the iodide/tri-iodide (I^-/I_3^-) electrolyte [33−35].

The sensitizers dye molecules are often covalently immobilized on the semiconductor metal oxide surfaces using carboxylic acid anchoring groups [36−38]. Recently, by exploiting the metal-ligand coordination chemistry of metalloporphyrins, an alternate method was established to the covalent immobilization of dye molecules [39]. Iron and nickel porphyrins have been extensively investigated for their metal-ligand coordination dynamics [40,41]. However, zinc-based porphyrins were chosen to be assembled on TiO_2 films by metal coordination for the following reasons. There is no ambiguity about the oxidation state, 2^+, of the zinc metal; it pref ers to form a five-coordinated complex by accepting only one axial ligand and the d orbitals of the Zn^{2+} are completely filled. Hence, zinc(II)-based porphyrin sensitizer was chosen as the representative metalloporphyrin, whereas phenylimidazole was used as the coordinating linker between the metalloporphyrin sensitizer and TiO_2 surface, because of its good rigid structure and a carboxyl acid anchoring group that bound to TiO_2. A key advantage of this modular assembly approach is that it allowed employing different sensitizers having different redox and spectral properties, and permitted us to verify their ability of photocurrent generation.

Herein, two metalloporphyrin-based photosensitizer molecules MP_A and MP_B (M = Zn, P=Tetrapyrrole) were adopted and grafted on the surface-modified TiO_2 NRs photoanode through the metal-ligand axial coordination assembly strategy. The ligand 4-carboxypyridine was utilized to decorate TiO_2 nanorods (NRs) and as the coordinating linker between the metalloporphyrin sensitizers (MP) and TiO_2. The MP_B molecule has D-π-A conjugated structure compared to the MP_A molecule. As-prepared MP_B/TiO_2 NRs array not only achieves a high current density, but also remarkably enhances the light absorption capacity. It is speculated that the interfacial electron transfer kinetics are critical to the enhancement of photocurrent signals. Therefore, the scanning photoelectrochemical microscopy (SPECM) and intensity modulated photocurrent spectroscopy (IMPS) were employed to systematically evaluate the continuous PET dynamics for the MP/TiO_2 NRs photoelectrode.

2. Experimental section

2.1. Regents and materials

Iodine gas (I_2) (Sigma-Aldrich, 99.9%), HCl (36.0%−38.0%), 4-carboxyphenylimidazole ($C_9H_8N_2O_2$, Aladdin, >99.9%) and tetrabutylammonium hexafluorophosphate ($C_{16}H_{36}F_6NP$, Aladdin, 96%) were purchased from Aladdin Chemistry Co. Tetrabutyl titanate ($C_{16}H_{36}O_4Ti$, Aladdin, 96%), tetrabutylammonium trifluoromethanesulfonate ($C_{17}H_{36}F_3NO_3S$, Alfa Aesar, 95%) and KI (Alfa Aesar, 95%) were obtained from Sinopharm Chemical Reagent Co. All chemicals were used in experiment without any further purification. All solutions were prepared with deionized Milli-Q water. The metal porphyrins A and B (Mark as MP_A and MP_B) were synthesized according to the method reported in previous literature [25].

2.2. Synthesis of MP/TiO_2 NRs film on FTO substrate

FTO glass substrates were first cleaned using soap and water, then immersed in acetone and deionized (DI) water followed by sonication for 30 min and 30 min, respectively, and then dried with N_2 gas. A thin 1D TiO_2 NRs layer was then deposited on the FTO surface by hydrothermal synthesis [42]. In a typical procedure, the solution containing 15 mL of DI water and 15 mL of HCl (36.0%−38.0%) was stirred for 10 min then, 500 μL of $C_{16}H_{36}O_4Ti$ was added. After vigorously stirring for another 10 min, the obtained mixture solution was poured into a 25 mL Teflon-lined stainless steels autoclave. Among, the FTO substrate was placed at an angle against the wall of the Teflon-liner and the conducting side facing downwards. The autoclave was kept at 150 °C for 5 h in the oven until the temperature dropped to room temperature, and the sample was taken out and rinsed with DI water. Finally, the TiO_2 NRs film was obtained after annealing in air at 500 °C for 1 h.

The MP/TiO_2NRs film was synthesized following the procedures shown in Fig. 1. Briefly, the TiO_2 NRs sample was firstly immersed in the 4-carboxyphenylimidazole ethanol solution for 12 h to decorate TiO_2 NRs film surface, and followed by rinsing with ethanol for removal of loose bonded group and drying at 130 °C. Then the surface-modified FTO/TiO_2 NRs electrode was again immersed in the metal porphyrin sensitizers dichloromethane solution (0.1 mmol·L^{-1}) for 4 h, and the unbound porphyrin sensitizers were removed by washing several times with DI water and dichloromethane, then dry in the air. The obtained photoanodes are named as MP_A/TiO_2 NRs and MP_B/TiO_2 NRs.

3. Results and discussion

3.1. Structure characterization

The method of assembling photosensitizer molecules on the electrode surface through highly oriented metal-ligand binding is a successful strategy to improve the photoelectric conversion efficiency. Herein, two metalloporphyrin-based photosensitizer molecules MP_A and MP_B (M = Zn, P=Tetrapyrrole) were prepared and the synthetic route is depicted in Fig. S1. The most critical step in this synthesis route is the introduction of an electron-donating diarylamino group (D) attached at the alkynyl π bridge opposite the meso-position of porphyrin core systematically. The molecular structures of the obtained photosensitizer molecules MP_A and MP_B are shown in Fig. 2A. The UV-vis absorption spectra and emission spectra of photosensitizer molecules MP_A and MP_B in CH_2Cl_2 solvent are shown in Fig. 2B. Both molecules MP_A and MP_B exhibit typical porphyrin characteristic absorption, However, MP_B exhibits a broad absorption peak, and the Soret and Q bands are shifted to longer wavelengths compared to MP_A, which is due to the introduction of the donor when coupling between the aromatic substituents and the porphyrin ring, and the expansion of the conjugate system in MP_B. This further illustrates the intramolecular charge transfer (ICT) transitions of D-A conjugate molecular MP_B.

To overcome the inherent weaknesses such as low carrier mobility and large bandgap of TiO_2, surface modification has been intensively studied. We designed a novel and facile strategy to construct supramolecular light-harvesting bodies on TiO_2 NRs arrays, that is, through the axial coordination of the central metal ion of zinc porphyrin with the imidazolyl groups on the

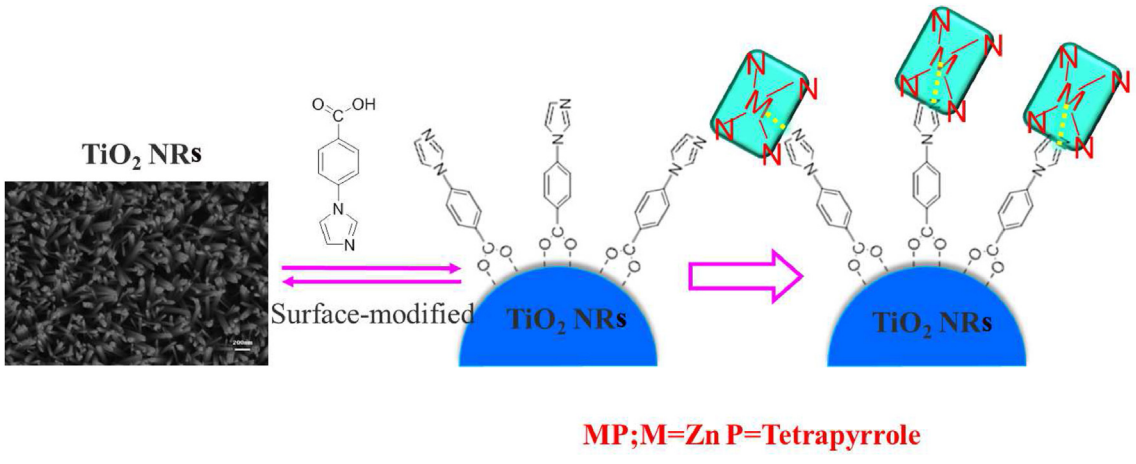

Fig. 1. Schematic illustration for the synthetic route of MP_A/TiO_2 NRs and MP_B/TiO_2 NRs photoanodes.

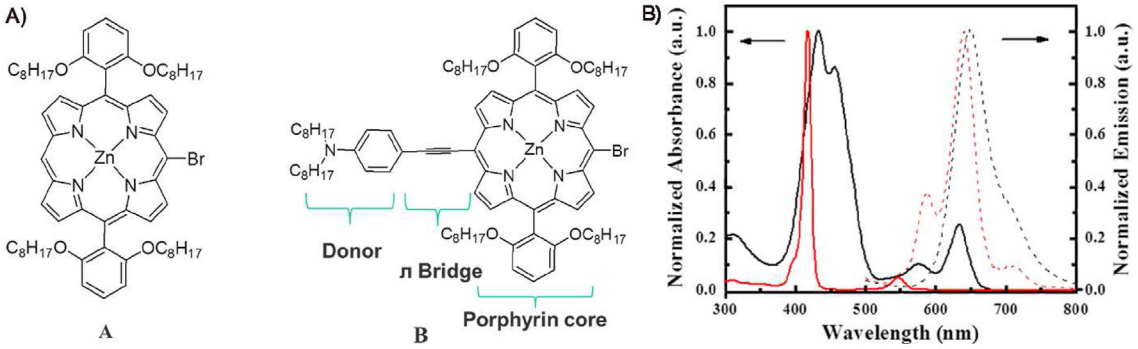

Fig. 2. (A) The molecular structures of MP_A and MP_B. (B) Normalized absorption (solid) and emission (dashed) spectra of MP_A (red) and MP_B (black) in CH_2Cl_2 solvent.

surface-modified TiO_2 NRs supports, forming the composite MP/TiO_2 NRs photoelectrode. The morphologies of TiO_2 NRs, MP_A/TiO_2 NRs and MP_B/TiO_2 NRs photoanodes were investigated by the field emission scanning electron microscope (FESEM). As shown in Fig. 3A, the well-aligned TiO_2 nanorods (TiO_2 NRs) array with an average length of 1.1 μm grown on the FTO glass substrate by the hydrothermal method. Fig. 3B is a high magnification image of the MP_A/TiO_2 NRs, which reveals that the entire surface of the FTO substrate was covered very uniformly with TiO_2 NRs, indicating that the addition of MP_A will not destroy the array of TiO_2 NRs. Notably, the morphology of MP_B/TiO_2 NRs is messier and clearly exhibit coarser surface morphology than that of TiO_2 NRs, which are preliminarily attributed to the decoration of MP_B (Fig. 3C).

The phase of the samples was determined by X-ray diffraction (XRD). As we all know, the FTO glass (F: SnO_2) is a transparent conductive fluorine-doped tin oxide substrate. Thence, FTO substrates have a tetragonal rutile phase of SnO_2 (JCPDS file No. 41−1445). For TiO_2 NRs film (Fig. 3D), the diffraction

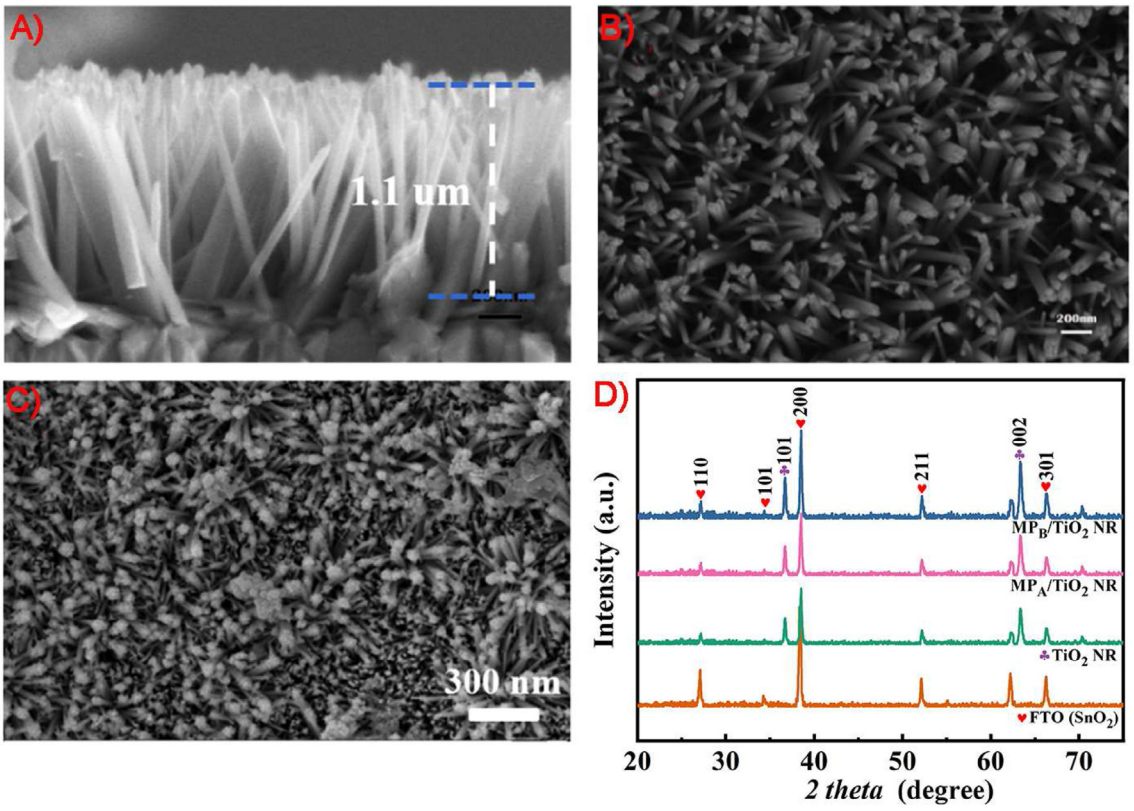

Fig. 3. (A-C) the scanning electron micrographs of cross-sectional views for (A) FTO/TiO_2 NRs, (B) MP/TiO_2 NRs and (C) MP/TiO_2 NRs. (D) the XRD patterns of FTO, FTO/TiO_2 NRs, MP_A/TiO_2 NRs and MP_B/TiO_2 NRs.

peaks at 36.1° and 63.2° could be well indexed to the (101) and (002) crystal planes of the tetragonal rutile phase (JCPDS file No. 21−1276), respectively [43]. This indicates that the TiO_2 NRs arrays are well crystallized throughout their length and the axis perpendicular to the substrate. The XRD patterns of the MP_A/TiO_2 NRs and MP_B/TiO_2 NRs exhibit no considerable difference from that of the pristine TiO_2 NRs, which was consistent with the poor crystallization of the modified photosensitizer molecules MP_A and MP_B, at the same time, it also explains the small amounts of MP_A and MP_B molecules being loaded on the modified TiO_2 NRs surface.

3.2. Optical properties and photoelectrochemical performances

Fig. 4A shows the UV-vis diffusion spectra of TiO_2 NRs, MP_A/TiO_2 NRs and MP_B/TiO_2 NRs samples in order to investigate the influence of light absorption. It is worth noting that the light absorption band edge is located at ca. 413 nm for TiO_2 NRs samples, which is stemmed from the bandgap photoexcitation of TiO_2 NRs [44]. However, porphyrin sensitizer molecule MP_A or MP_B is covalent fixation on the TiO_2 NRs surface to influence the optical property of TiO_2. The spectra of MP/TiO_2 NRs and MP/TiO_2 NRs display obvious red-shift of absorption edge and extend to the visible region compared with that of the pristine TiO_2 NRs, revealing a better light absorption ability, which is due to the presence of metalloporphyrin groups to effectively enhance the light absorption capacity. The MP_B/TiO_2 NRs sample has a wider visible light absorption range because aniline was introduced into the molecular B structure as a donor, and the intermediate π-bridge between the donor aniline and the acceptor porphyrin ring was used to form an effective D-π-A structure, which broadens the absorption in the visible region and allows a proper electron distribution on the highest occupied molecular orbital (HOMO) and lowest unoccupied molecular orbital (LUMO), effectively facilitating charge separation and reducing charge recombination. The inset photographs in Fig. 4A present the prepared TiO_2 NRs, MP_A/TiO_2 NRs and MP_B/TiO_2 NRs electrodes. It can be seen that the three electrodes have different colors, proving the successful preparation of these electrodes.

The PEC performance of the MP_B/TiO_2 NRs films was evaluated in 0.5 $mol \cdot L^{-1}$ Na_2SO_4 solution under AM 1.5 G illumination. For comparison, the pristine TiO_2 NRs and MP_A/TiO_2 NRs films were also measured under the same conditions. All the applied potentials versus Ag/AgCl have been converted to the corresponding potentials versus RHE. Fig. 4B illustrates the photoinduced linear sweep voltammetric (LSV) curves of TiO_2 NRs, MP_A/TiO_2 NRs and MP_B/TiO_2 NRs photoanode. It could be seen that the photocurrents induced from the photoelectrodes all present a gradually rising trend when the sweep voltage gradually increases from negative to positive. The current density of the FTO/TiO_2 NRs photoanode increased slowly in dark conditions but increased significantly in light. In addition, the MP_B/TiO_2 NRs electrode exhibited much better PEC performance than the TiO_2 NRs and MP_A/TiO_2 NRs electrodes. The starting potential was 0.15 V and slowly increased after 0.8 V. The MP_B/TiO_2 NRs electrode produced a photocurrent density of 1.21 $mA \cdot cm^{-2}$ at 1.23 V, which are 2 and 1.35 times those of TiO_2 NRs and MP_A/TiO_2 NRs electrodes, respectively, indicating that TiO_2 NRs and the porphyrin B molecules have very good matching energy levels, which promotes charge separation

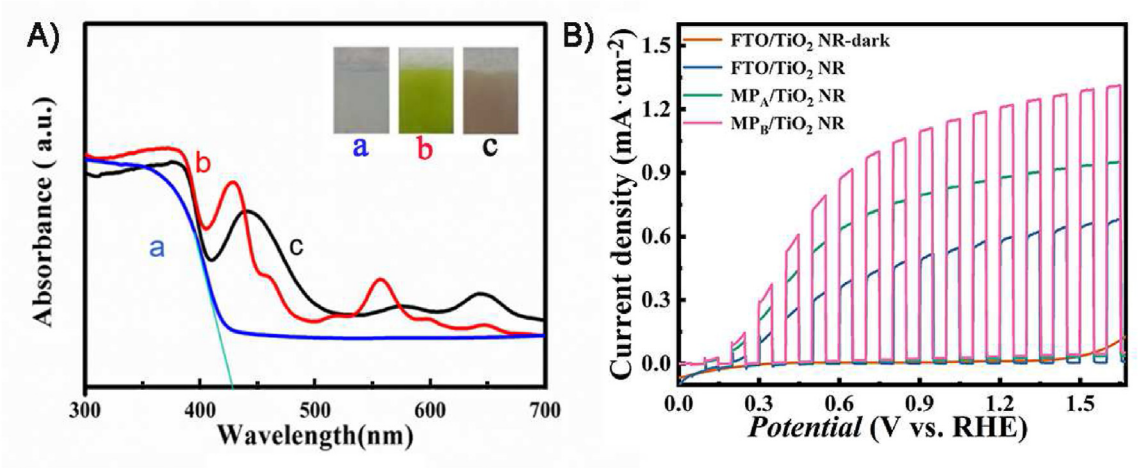

Fig. 4. (A) The UV-vis diffusion reflectance spectra of FTO/TiO_2 NRs (a), MP_A/TiO_2 NRs (b) and MP_B/TiO_2 NRs (c), and the insets are photos of the corresponding electrodes. (B) LSV curves of FTO/TiO_2 NRs in dark, FTO/TiO_2 NRs, MP_A/TiO_2 NRs and MP_B/TiO_2 NRs under AM 1.5G 100 $mW \cdot cm^{-1}$.

and enhances light capture. An additional reason for the increased photocurrent density of the MP_B/TiO_2 NRs electrode is the presence of an electron-pushing group (alkoxy chain) in the MP_B molecule, which promotes charge transfer within the porphyrin MP_B molecule and accelerates photogenerated electron transfer. The photo response capability and stability of all the photoanodes were investigated by current-time curves at 1.23 V vs. RHE under chopped light illumination. As displayed in Fig. S3B, the as-prepared photoanodes show fast photocurrent responses when the light switches on. Gratifyingly, the MP_B/TiO_2 NRs photoanode still exhibits the highest photocurrent density without noticeable decline. The highest photocurrent of about 3.5 $mA \cdot cm^{-2}$ was obtained. Amperometric *i-t* curves were recorded to research the stability of the catalyst (Fig. S2A). During the 1900s of PEC measurements, all of the samples retained relatively good stability, and no observable color change occurred on the material during the electrolysis (Fig. S2B).

3.3. Mechanism analysis

To figure out the reason for the enhanced PEC properties of MP_B/TiO_2 NRs, the band structures of MP_A, MP_B and TiO_2 NRs were firstly studied. The HOMO and LUMO levels of MP_A and MP_B can be determined by cyclic voltammetry (CV), which is shown in Fig. S3, and the data are summarized in Table S1. The HOMO values of MP_A, MP_B were close to each other and found to be −3.22 eV and −3.026 eV, respectively. The conduction band energy (E_{CB}) of TiO_2 is −4.4 eV at vacuum energy levels according to the literature. The LUMO levels of MP_A and MP_B are significantly lower than the conduction band edge energy level of the TiO_2 electrode in Fig. 5A, indicating that the electron injection process is energetically favorable, providing the greater driving force for electron injection from MP_A or MP_B to TiO_2. Additionally, The HOMO values of MP_A and MP_B were reported to be higher than the energy level of I_3^-/I^- (−4.58 eV) [39]. It suggests that the MP_A and MP_B sensitizers could thermodynamically accept the released electrons from I^- to I_3^- process. Thus, the schematic diagram of the photoexcited electron transfer process for the MP_B/TiO_2 NRs photoanode under light irradiation is displayed in Fig. 5B. In detail, under the irradiation of visible light, TiO_2 NRs can effectively absorb visible light, and produce a large number of photogenerated electron-hole pairs. The photogenerated electrons on CB of TiO_2 NRs are transferred to SPECM probe, and can react with the generated I_3^- to form I^- by reduction reaction. The probe molecule, I^-, is oxidized to I_3^- at the substrate probe. This process is repeated, and thus improves the PEC performance of the MP_B/TiO_2 NRs photoanode.

To gain an in-depth understanding into the charge transfer mechanism in MP_B/TiO_2 NRs photoanode, the electrochemical impedance spectra (EIS) have been measured to understand the charge transfer of all photoanodes in more detail. Based on a previous report, the smaller the semicircle diameter, the better carrier transmission characteristics and better interface charge transport kinetics [45]. As shown in Fig. 6A, compared with the TiO_2 NRs and MP_A/TiO_2 NRs, the MP_B/TiO_2 NRs photoanode shows the smallest radius, which could be contributed to the role of the donor-acceptor conjugated structure in the MP_B molecule to provide continuous electron transfer, accelerating the separation of photogenerated holes. Therefore, it is suggested that the conjugated molecules of D-A structure play an important role in improving the transportation of photogenerated charges.

To further unveil the underlying mechanism for the enhanced PEC of MP_B/TiO_2 NRs photoanode, the intensity modulated photocurrent spectroscopy (IMPS) was used to estimate the PET lifetime from

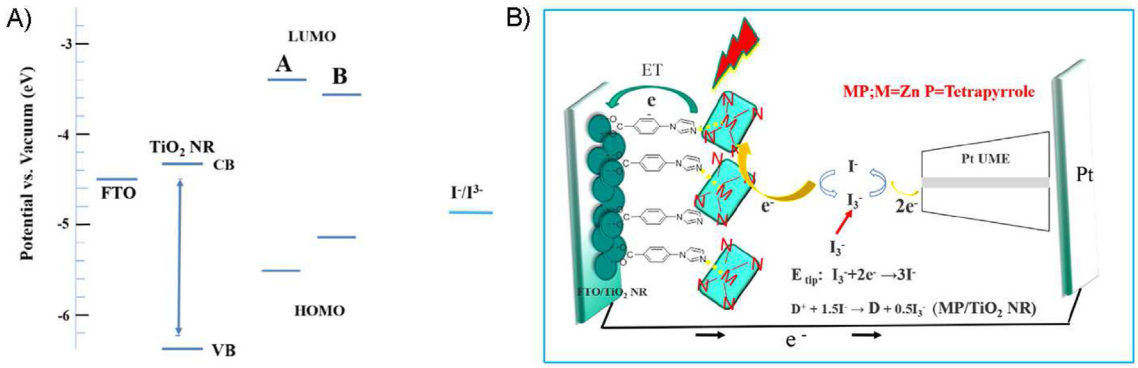

Fig. 5. (A) Energy level (eV) plot of HOMO and LUMO molecular orbitals for MP_A, MP_B sensitizers and TiO_2. (B) Schematic diagram of the photoexcited electron transfer process for the MP_B/TiO_2 NRs photoanode under light irradiation.

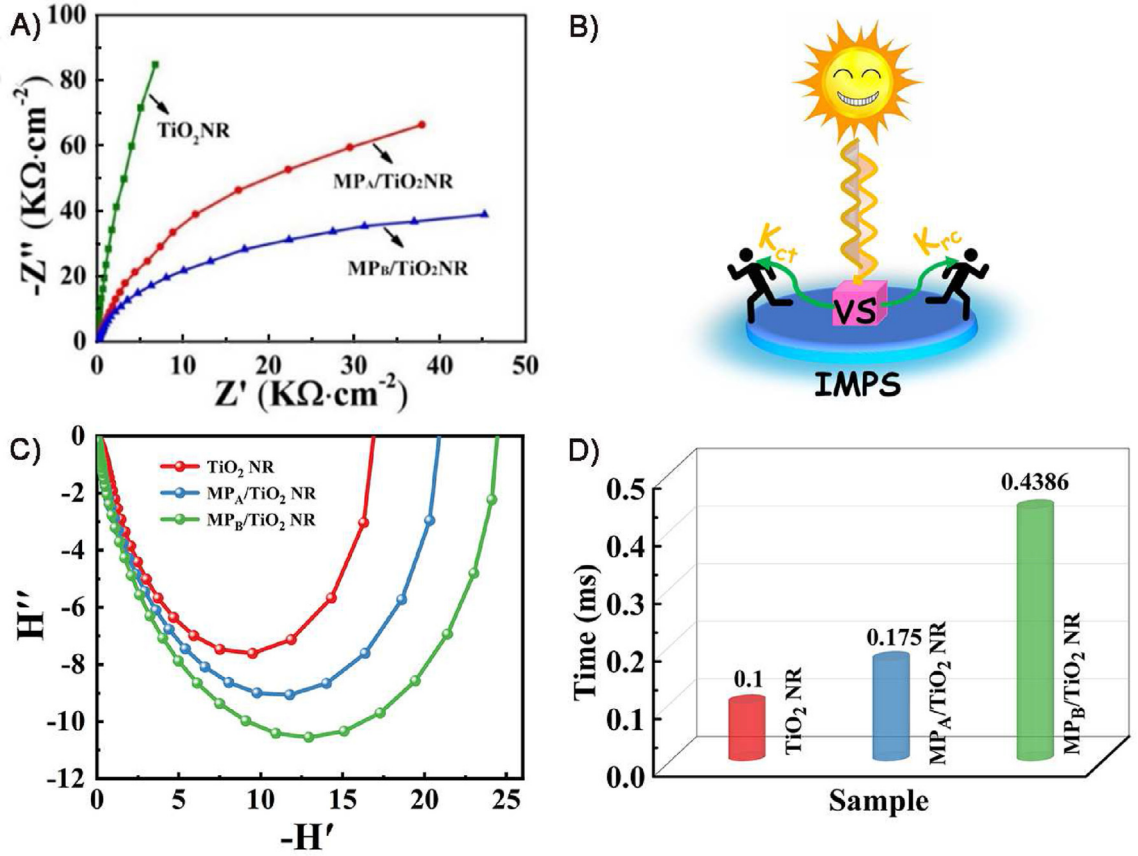

Fig. 6. (A) Electrochemical impedance spectra of TiO_2 NRs, MP_A/TiO_2 NRs and MP_B/TiO_2 NRs photoanodes. (B) Principle of the IMPS setup. (C) Intensity modulated photocurrent spectra and (D) transit time plots of TiO_2NRs, MP_A/TiO_2 NR and MP_B/TiO_2 NRs photoanodes.

the equation $\tau_d = (2\pi f_{min})^{-1}$ (Fig. 6B) [46], where τ_d is the transition time and f_{min} is the characteristic minimum frequency. The transition time represents the velocity of PET across the fixed distance, implying the recombination possibility of electron and hole [47]. Fig. 6C shows the IMPS analysis data of TiO_2 NRs, MP_A/TiO_2 NRs and MP_B/TiO_2 NRs photoanodes. The order of τ_d values is as follows: MP_B/TiO_2 NRs (0.4386 ms) > MP_A/TiO_2 NRs (0.175 ms) > TiO_2 NRs (0.1 ms) (Fig. 6D). Therefore, the average photoinduced electron transfer time (τ_d) estimated from the lowest imaginary part frequency is longer for the MP_B/TiO_2 NRs photoanode, which is due to the push-pull conjugated structure of MP_B molecular to modulate the continuous migration of electrons from MP_B molecule to TiO_2 substrate. In detail, the modification of MP_B molecule on TiO_2 NRs surface via axial coordination of metal ligands porphyrins mainly improves the continuous photoinduced electron transfer efficiency, resulting in a higher photoelectron density in MP_B/TiO_2 NRs, however, taking into account the low conductivity of porphyrin-base organic semiconductors, higher electron concentration will increase the repulsion between electrons, thereby, prolonging the time that electrons pass through the TiO_2 NRs film to the backside of the FTO. Although more time is needed to collect electrons, the number of electrons reaching the back of the electrode increases, resulting in high photocurrent, which is consistent with the abovementioned measured photocurrent analysis results.

For gaining deep insights into the electron migration process and PET dynamics information on the TiO_2 NRs surface assembled with metalloporphyrin-based photosensitizer molecules, the self-construction SPECM platform was adopted to *in situ* quantitatively investigate the "fast" and "slow" electron transfer dynamics for different integrated systems interfaces [48–50] (Fig. 7A). Firstly, the cyclic voltammetric curve was recorded in the electrolyte of 1.1 mmol·L^{-1} I_3^- and 0.1 mol·L^{-1} TBAS to evaluate Pt ultramicroelectrode (UME). Subsequently, in the four-electrode system, the different probe approach curves were recorded by tip current-distance relationships for the various substrates under light illumination (Fig. 7B). Typically, SPECM probe current presented an increasing trend as the tip approached the different surfaces of photoanodes (TiO_2 NRs, MP_A/TiO_2 NRs and MP_B/TiO_2 NRs)

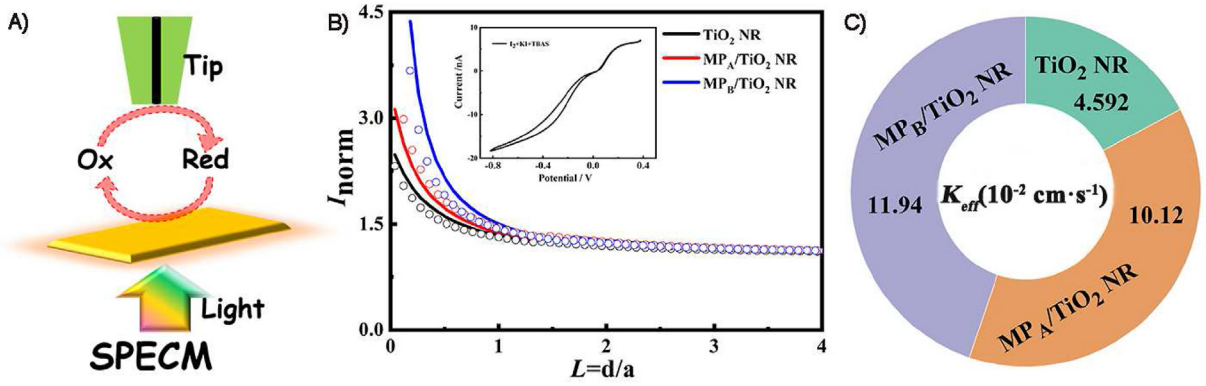

Fig. 7. (A) Principle of the SPECM setup, (B) probe approach curves, and (C) rate constant (K_{eff}) plot at a Pt UME (RG = 4) toward different films surfaces under UV-vis illumination. The inset in (B) shows the cyclic voltammograms of Pt UME in 1.1 mmol·L^{-1} I_3^- + 0.1 mol·L^{-1} TBAS acetonitrile solutions at scan rate 50 mV·s^{-1}.

under visible-light irradiation, which is called "positive feedback" phenomenon. This phenomenon was attributed to that photogenerated electrons can be prone to take part in the reduction reaction of I_3^- to I^- in the novel charge transfer channel. However, it is worth mentioning that the magnitude of the positive feedback was highest in the case of the MP_B/TiO_2 NRs substrates. In detail, the probe molecule, I^-, is oxidized to I_3^- at the substrate, and the generated I_3^- is reduced to I^- at the SPECM probe. In this way, the process is reciprocated to get highest positive feedback approach curves. Among, the I_3^-/I^- redox couple not only was regarded as the probe molecule of quantitative analysis, but also as a scavenger, which can effectively improve the separation efficiency of the photo-generated charge in the interface.

Coupled with data fitting, the kinetic rate constant (K_{eff}) values for different samples can be obtained through the previous theoretical model equations and the theoretical simulation for the PET kinetics is introduced in detail (S Equations (1)−(5)). In Fig. 7B, it is found that the K_{eff} was performed in the following order: MP_B/TiO_2 NRs > MP_A/TiO_2 NRs > TiO_2 NRs. The value of K_{eff} is 11.94 × 10^{-2} cm·s^{-1} for MP_B/TiO_2 NRs, which is about 2.6 times higher than that of pure TiO_2 NRs (4.592 × 10^{-2} cm·s^{-1}). This fast electron transfer kinetics of MP_B/TiO_2 NRs can be attributed to intramolecular charge transfer (ICT) transitions of D-A conjugate molecular MP_B compared to MP_A/TiO_2 NRs, Similarly, the push-pull type structure of MP_B molecule contributes to the transport of electrons.

Light is the sole driving force for the charge transfer across the substrate/electrolyte interface. Therefore, the impact of studying light wavelength and illumination intensity on MP_B/TiO_2 NRs substrates PET dynamics are essential. SECM approach curves were recorded at various wavelengths ranging from 419 to 515 nm as shown in Fig. 8A. It is found that the "positive feedback" is observed at wavelengths of 469, 487, 515, 546, and 531 nm, and meanwhile the "negative feedback" is seen at wavelength of 419 nm. The probe current will be decreased under dark condition called negative feedback, because the photogenerated electrons are hard to participate in the reduction reaction of I_3^- to I^-. Similarly, the same simulating processes are performed to give the rate constant (k_{eff}) at specific light wavelengths and the values are summarized in Fig. 8B. It is observed that the highest PET rate (k_{eff}) for the MP_B/TiO_2 NRs material is mainly presented at 531 nm. Interestingly, the wavelength of 531 nm is well matched with the strongest DRS absorption range of MP_B/TiO_2 NRs (Fig. 4A). It has been proved that undoubtedly the photoinduced electron transfer kinetics by SECM measurement can truly and effectively evaluate the fast and slow behaviors of electronic transmission at the electrode micro interface.

In addition, we also investigated the effect of light intensity on the regular probe approach curve. Probe approach curves for MP_B/TiO_2 NRs substrates were recorded at different intensities and are shown in Fig. 8C. These probe approach curves all show the positive feedback phenomenon when illumination intensity was varied from the lowest of 20% to the highest of 100%. The tip current magnitude was greater under the light intensity of 80%. According to the data fitting, the quantitative kinetics results revealed that the large rate constant (k_{eff}) could be achieved as show in Fig. 8D. Importantly, the highest k_{eff} value for MP_B/TiO_2 NRs was achieved at the light intensity of 80%. The results demonstrated that the light intensity is not the only factor that influences the k_{eff} and the blind strengthening of the illumination intensity is not always to accelerate the electron transfer rate, further demonstrating that the material exhibiting greater k_{eff} value at a particular

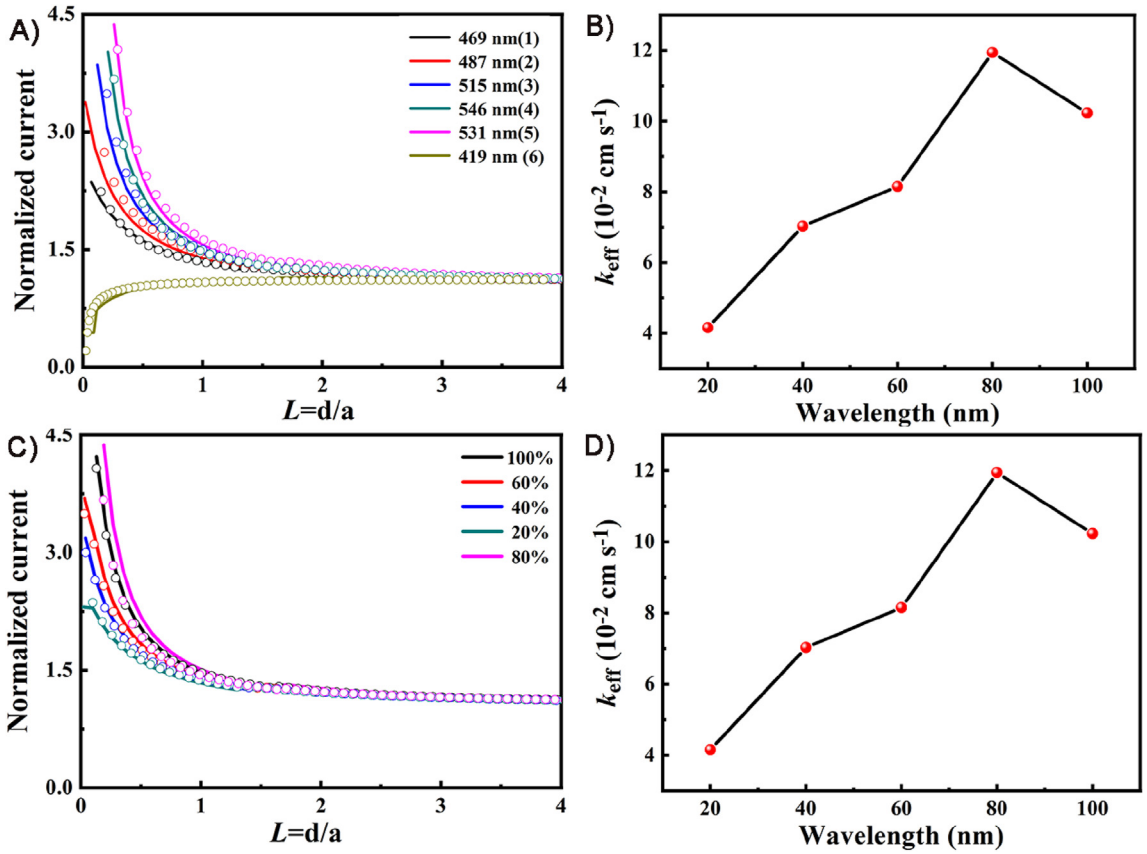

Fig. 8. (A) SECM probe approach curves of MP_B/TiO_2 NRs-modified electrodes under different wavelengths. (B) Dependence of k_{eff} on light wavelength. (C) SECM approach curves of MP_B/TiO_2 NRs-modified electrodes at different light intensities. (D) Dependence of k_{eff} on light intensity.

intensity is considered to be the better photocatalyst.

4. Conclusions

In this work, we have successfully assembled the metalloporphyrin-based photosensitizer molecules (MP) on the TiO_2 NRs-modified surface by using a coordination ligand method. The resulted unique MP_B/TiO_2 NRs photoelectrode displayed the significantly improved photocurrent density of 1.23 $mA \cdot cm^{-2}$, which is 2.41 times higher than the pristine TiO_2 NRs. Such a remarkable photocurrent density for the MP_B/TiO_2 NRs could be attributed to the conjugated molecules MP_B of D-A structure which can effectively accelerate the PET process. The photoexcited electron migration behavior and accumulation were visualized through SPECM. Simultaneously, the electron-transfer kinetic rate constant (K_{eff}) of MP_B/TiO_2 NRs was obtained to be 11.94 $\times$ 10^{-2} $cm \cdot s^{-1}$ under visible light illumination. Furthermore, the rate constant of electron transfer reached the maximum at a wavelength of 531 nm with an illumination intensity of 80% for MP_B/TiO_2 NRs, which further reveals that the PET behavior is the prime source for the enhanced photocurrent density. In a word, it is expected to provide new thread for gaining deep insight into the mechanism of the PET process for the metal-ligand coordination of metalloporphyrins and to optimize the PEC performance.

Acknowledgements

We are thankful to the National Natural Science Foundation of China (22174110 and 22127803), the Industrial Support Plan of Gansu Provincial Department of Education (2021cyzc-01), and the Special Fund Project for Guiding Local Scientific and Technological Development by the Central Government (2020-2060503-17).

References

[1] Cao H Y, Wang T T, Li J X, Wu J B, Du P W. A molecular cobaloxime cocatalyst and ultrathin FeOOH nanolayers Co-modified $BiVO_4$ photoanode for efficient photo-electrochemical water oxidation[J]. J. Energy Chem., 2022, 69: 497−505.

[2] Gao L L, Li F, Hu H G, Long X F, Xu N, Hu Y P, Wei S Q, Wang C L, Ma J T, Jin J. Dual modification of a $BiVO_4$

photoanode for enhanced photoelectrochemical performance[J]. ChemSusChem., 2018, 11(15): 2502−2509.

[3] Zhang B Y, Liu K W, Xiang Y, Wang J M, Lin W R, Guo M, Ma G J. Facet-oriented assembly of Mo:$BiVO_4$ and Rh:$SrTiO_3$ particles: integration of P-N conjugated photoelectrochemical system in a particle applied to photocatalytic overall water splitting[J]. ACS Catal., 2022, 12(4): 2415−2425.

[4] Mitsui M, Nakagome Y, Niihori Y, Inoue S, Fujiwara Y, Kobayashi K. Starburst-shaped D-π-A chromophores possessing a hexaethynylbenzene core for dye-sensitized solar cells[J]. ACS Appl. Mater. Interfaces., 2021, 13(30): 35739−35749.

[5] Chang P H, Sil M C, Reddy K SK, Lin C H, Chen C M. Polyimide-based covalent organic framework as a photocurrent enhancer for efficient dye-sensitized solar cells[J]. ACS Appl. Mater. Interfaces., 2022, 14(22): 25466−25477.

[6] Li F S, Yang H, Zhuo Q M, Zhou D H, Wu X J, Zhang P L, Yao Z Y, Sun L C. A cobalt@cucurbit[5]uril complex as a highly efficient supramolecular catalyst for electrochemical and photoelectrochemical water splitting[J]. Angew. Chem. Int. Ed., 2021, 60(4): 1976−1985.

[7] Lu Y, Yang Y L, Fan X Y, Li Y Q, Zhou D H, Cai B, Wang L Y, Fan K, Zhang K. Boosting charge transport in $BiVO_4$ photoanode for solar water oxidation[J]. Adv. Mater., 2022, 34(8): e2108178.

[8] Sahu T K, Alam S, Bhowmick S, Mohanta M K, Qureshi M. Phosphorus nitride nano-dots as a versatile and metal-free support for efficient photoelectrochemical water oxidation [J]. Chem. Commun., 2021, 57(50): 6157−6160.

[9] Song Y R, Zhang X M, Zhang Y X, Zhai P L, Li Z W, Jin D F, Cao J Q, Wang C, Zhang B, Gao J F, Sun L C, Hou J G. Engineering MoO_x/Mxene hole transfer layers for unexpected boosting photoelectrochemical water oxidation[J]. Angew. Chem. Int. Ed., 2022, 61(16): e202200946.

[10] Tateno H, Chen S Y, Miseki Y, Nakajima T, Mochizuki T, Sayama K. Photoelectrochemical oxidation of glycerol to dihydroxyacetone over an acid-resistant Ta:$BiVO_4$ photoanode[J]. ACS Sustain. Chem. Eng., 2022, 10(23): 7586−7594.

[11] Abdelkarim O, Selopal G S, Suresh K, Navarro-Pardo F, Kumar P, Ghuman K K, Yurtsever A, Bassioni G, Wang Z M, Rosei F. Role of surface engineering of hybrid structure for high performance quantum dots based photoelectrochemical hydrogen generation[J]. Chem. Eng. J., 2022, 429: 132425.

[12] Yu Z R, Guo H, Sun Z L, Li Y, Liu Y H, Yang W G, Zhu M Y, Jin H M, Li Y, Feng L Y, Li S, Prucnal S, Li W X. U7Co 3d impurity energy level mediated photogenerated carriers transfer in Bi_2S_3/ZnS:Co/TiO_2 photoanode[J]. Chem. Eng. J., 2022, 433: 134458.

[13] Shen Z, Song J, Yung B C, Zhou Z, Wu A, Chen X. Cancer therapy: merging strategies of cancer therapy based on ferroptosis [J]. Adv. Mater., 2018, 30(12): 1870084.

[14] Banerjee R, Furukawa H, Britt D, Knobler C, O'Keeffe M, Yaghi O M. Control of pore size and functionality in isoreticular zeolitic imidazolate frameworks and their carbon dioxide selective capture properties[J]. J. Am. Chem. Soc., 2009, 131(11): 3875−3877.

[15] Zhang G H, Chen J H, Yan H G, Su B, He X, Ran M. Effects of artificial aging on microstructure and mechanical properties of the Mg-4.5Zn-4.5Sn-2Al alloy[J]. J. Alloys Compd., 2014, 592: 250−257.

[16] Park J, Lee T H, Kim C, Lee S A, Choi M J, Kim H, Yang J W, Lim J, Jang H W. Hydrothermally obtained type-II heterojunction nanostructures of In_2S_3/TiO_2 for remarkably enhanced photoelectrochemical water splitting[J]. Appl. Catal. B Environ., 2021, 295: 120276.

[17] Wang S B, Liu P J, Meng C Z, Wang Y D, Zhang L, Pan L, Yin Z, Tang N, Zou J J. Boosting photoelectrochemical water splitting by Au@Pt modified ZnO/Cds with synergy of Au-S bonds and surface plasmon resonance[J]. J. Catal., 2022, 408: 196−205.

[18] Zhang M, Li F Y, Benetti D, Nechache R, Wei Q, Qi X W, Rosei F. Ferroelectric polarization-enhanced charge separation in quantum dots sensitized semiconductor hybrid for photoelectrochemical hydrogen production[J]. Nano Energy, 2021, 81: 105626.

[19] Kudo A, Miseki Y. Heterogeneous photocatalyst materials for water splitting[J]. Chem. Soc. Rev., 2009, 38(1): 253−278.

[20] Ding C M, Shi J Y, Wang Z L, Li C. Correction to photoelectrocatalytic water splitting: significance of cocatalysts, electrolyte, and interfaces[J]. ACS Catal., 2017, 7(3). 1706-1706.

[21] Feng Y C, Wang X, Wang Y Q, Yan H J, Wang D. *In situ* characterization of electrode structure and catalytic processes in the electrocatalytic oxygen reduction reaction[J]. J. Electrochem., 2022, 28(3): 2108531.

[22] Li Z L, Fang H, Chen Z P, Zou W X, Zhao C X, Yang X F. Regulating donor-acceptor interactions in triazine-based conjugated polymers for boosted photocatalytic hydrogen production[J]. Appl. Catal. B: Environ., 2022, 312: 121374.

[23] Han J, Li N J, Chen D Y, Xu Q F, Lu J M. Boosting photocatalytic activity for porphyrin-based D-a conjugated polymers via dual metallic sites regulation[J]. Appl. Catal. B: Environ., 2022, 317: 121724.

[24] Zou R Q, Sakurai H, Xu Q. Preparation, adsorption properties, and catalytic activity of 3d porous metal-organic frameworks composed of cubic building blocks and alkali-metal ions[J]. Angew. Chem. Int. Ed., 2006, 45: 2542−2546.

[25] Lu F T, Zhang J, Zhou Y Z, Zhao Y M, Zhang B, Feng Y Q. Novel D-π-A porphyrin dyes with different alkoxy chains for use in dye-sensitized solar cells[J]. Dyes and Pigments, 2016, 125: 116−123.

[26] Li S Z, Zhang S Y, Mei S, Kong X F, Yang M, Wu W J, Zhang S H, Tan H J. A novel porphyrin dye with phenoxazine as donor unit for efficient dye-sensitized solar cells[J]. Dyes and Pigments, 2021, 190: 109308.

[27] Zhou P J, Liang J Y, Lin B B, An Z W, Chen R, Chen X B, An Q, Chen P. Effect of the spatial configuration of donors on the photovoltaic performance of double D-π-A organic dyes[J]. ACS Appl. Mater. Interfaces., 2021, 13(34): 40648−40655.

[28] Chen Y Y, Tang Y Y, Zou J Z, Zeng K W, Baryshnikov G, Li C J, Xie Y S. Fluorenyl indoline as an efficient electron donor for concerted companion dyes: Enhanced light-harvesting and photocurrent[J]. ACS Appl. Mater. Interfaces., 2021, 13(42): 49828−49839.

[29] Grobelny A, Shen Z, Eickemeyer F T, Antariksa N F, Zapotoczny S, Zakeeruddin S M, Gratzel M. Molecularly tailored photosensitizer with an efficiency of 13.2% for dye-sensitized solar cells[J]. Adv. Mater. 2022: e2207785.

[30] Ji J M, Lee H J, Zhou H, Eom Y K, Kim C H, Kim H K. Influence of the Pi-bridge-fused ring and acceptor unit extension in D-π-A structured organic dyes for highly efficient dye-sensitized solar cells[J]. ACS Appl. Mater. Interfaces., 2022, 14(47): 52745−52757.

[31] Lv S X, Wu Y C, Cai K M, He H, Li Y J, Min L, Chen X S, Cheng J J, Yin L C. High drug loading and sub-quantitative loading efficiency of polymeric micelles driven by donor-receptor coordination interactions[J]. J. Am. Chem. Soc., 2018, 140(4): 1235−1238.

[32] Yen Y S, Chou H H, Chen Y C, Hsu C Y, Lin J T. Recent developments in molecule-based organic materials for dye-sensitized solar cells[J]. J. Mater. Chem., 2012, 22(18): 8734−8747.

[33] Engel Y, Elnathan R, Pevzner A, Davidi G, Flaxer E, Patolsky F. Cover picture: supersensitive detection of explosives by silicon nanowire arrays[J]. Angew. Chem. Int. Ed., 2010, 49(38): 6685.

[34] Hong S H, Wang Y F, Pan T Y, Chang C W, Kuo H H, Kuo M Y, Diau W G, Lin C Y, Wang C L, Lan C M. Enveloping porphyrins for efficient dye-sensitized solar cells[J]. Energy Environ. Sci., 2012, 5: 6933−6940.

[35] Li Y X, Wang G Y, Feng X X, Jia Q F, Li Y Y, Liu J L, Cao J, Liu J C. Double-layer novel zinc porphyrin based on axial coordination self-assembly for dye-sensitized solar cells[J]. J. Mol. Struct., 2021, 1242: 130819.

[36] Bassil B S, Dickman M H, Romer I, von der Kammer B, Kortz U. The tungstogermanate $[Ce_{20}Ge_{10}W_{100}O_{376}(OH)_4(H_2O)_{30}]^{56-}$: a polyoxometalate containing 20 cerium(iii) atoms[J]. Angew. Chem. Int. Ed., 2007, 46(32): 6192−6195.

[37] Li F, Wang Z Y, Stein A. Cover picture: shaping mesoporous silica nanoparticles by disassembly of hierarchically porous structures[J]. Angew. Chem. Int. Ed., 2007, 46(11). 1749-1749.

[38] Ragoussi M E, Cid J J, Yum J H, de la Torre G, Di Censo D, Grätzel M, Torres T. Carboxyethynyl anchoring ligands: a means to improving the efficiency of phthalocyanine-sensitized solar cells[J]. Angew. Chem. Int. Ed., 2012, 124(18): 4451−4454.

[39] Sakamoto K, Yoshino S, Takemoto M, Furuya N. Syntheses of near infrared absorbed phthalocyanines to utilize photosensitizers[J]. J. Porphyr. Phthalocyanines, 2013, 17: 605−627.

[40] Beale A M, Jacques S, Gibson E K, Michiel M. Progress towards five dimensional diffraction imaging of functional materials under process conditions[J]. Coord. Chem. Rev., 2014, 277−278: 208−223.

[41] Retsek J L, Drain C M, Kirmaier C, Nurco D J, Medforth C J, Smith K M, Sazanovich I V, Chirvony V S, Fajer J, Holten D. Photoinduced axial ligation and deligation dynamics of nonplanar nickel dodecaarylporphyrins[J]. J. Am. Chem. Soc., 2003, 125(32): 9787.

[42] Zheng X L, Dinh C T, de Arquer F P, Zhang B, Liu M, Voznyy O, Li Y Y, Knight G, Hoogland S, Lu Z H, Du X W, Sargent E H. $ZnFe_2O_4$ leaves grown on TiO_2 trees enhance photoelectrochemical water splitting[J]. Small, 2016, 12(23): 3181−3188.

[43] Guo K Y, Liu Z F, Zhou C L, Han J H, Zhao Y F, Liu Z C, Li Y J, Cui T, Wang B, Zhang J. Fabrication of TiO_2 nano-branched arrays/Cu_2S composite structure and its photoelectric performance[J]. Appl. Catal. B: Environ., 2014, 154155: 27−35.

[44] Li S, Mo Q L, Zhu S C, Wei Z Q, Tang B, Liu B J, Liang H, Xiao Y, Wu G, Ge X Z, Xiao F X. Unleashing insulating polymer as charge transport cascade mediator[J]. Adv. Funct. Mater., 2022, 32(30): 2110848.

[45] Wu J, Huang P, Fan H T, Wang G, Liu W S. Metal-organic framework-derived P-Cu_2O/N-Ce-Fe_2O_3 heterojunction nanorod photoanode coupling with a FeOOH cocatalyst for high-performance photoelectrochemical water oxidation[J]. ACS Appl. Mater. Interfaces., 2020, 12(27): 30304−30312.

[46] Kruger J, Plass R, Gratzel M, Cameron P J, Peter L M. Charge transport and back reaction in solid-state dye-sensitized solar cells: study using intensity-modulated photovoltage and photocurrent spectroscopy[J]. J. Phys. Chem. B., 2003, 107(31): 7536−7539.

[47] Salant A, Shalom M, Tachan Z, Buhbut S, Zaban A, Banin U. Quantum rod-sensitized solar cell: Nanocrystal shape effect on the photovoltaic properties[J]. Nano lett, 2012, 12(4): 2095−2100.

[48] Ning X M, Li W Q, Meng Y, Qin D D, Chen J, Mao X, Xue Z H, Shan D L, Devaramani S, Lu X Q. New insight into procedure of interface electron transfer through cascade system with enhanced photocatalytic activity[J]. Small, 2018, 14(15): e1703989.

[49] Ning X M, Lu B Z, Zhang Z, Du P Y, Ren H X, Shan D L, Chen J, Gao Y J, Lu X Q. An efficient strategy for boosting photogenerated charge separation by using porphyrins as interfacial charge mediators[J]. Angew. Chem. Int. Ed., 2019, 58(47): 16800−16805.

[50] Ning X M, Yin D, Fan Y P, Zhang Q, Du P Y, Zhang D X, Chen J, Lu X Q. Plasmon-enhanced charge separation and surface reactions based on Ag-loaded transition-metal hydroxide for photoelectrochemical water oxidation[J]. Adv. Energy Mater., 2021, 11(17): 2100405.

通过扫描光电化学显微镜研究超分子光敏剂-二氧化钛薄膜系统的光诱导电子转移

张生雅，姚敏，王泽，刘天娇，张蓉芳，叶慧琴，冯彦俊，卢小泉*
西北师范大学化学化工学院，甘肃省生物电化学与环境分析重点实验室，甘肃 兰州 730030

摘要

在基于 TiO_2 的光阳极上枝接电荷转移通道仍然是太阳能到化学转换技术的一个迫切瓶颈。尽管进行了大量的尝试，但 TiO_2 作为有前途的光阳极材料仍然受到电荷传输动力学迟缓的影响。因此，一种组装策略涉及将金属卟啉基光敏剂分子（MP）轴向配位嫁接到表面改性的 TiO_2 纳米棒（TiO_2 NRs）光阳极上，形成复合 MP/TiO_2 NRs 光电极。正如预期的那样，与单独的 TiO_2 NR 和 MPA/TiO_2 NRs 光电极相比，所得到的独特的 MPB/TiO_2 NRs 光电极具有明显提高的光电流密度。采用扫描光电化学显微镜（SPECM）和强度调制光电流光谱（IMPS）系统地评估了 MP/TiO_2 NRs 光电极的连续光激发电子转移（PET）动力学信息。通过数据拟合发现，在光照条件下，MPB/TiO_2 NRs 的光电子转移速率（k_{eff}）常数比纯 TiO_2 NRs 高 2.6 倍左右。MPB/TiO_2 NRs 的高动力学常数是由于 D-A 结构的共轭分子 MPB 可以有效地加速分子内电子转移，以及促进电子在新型电荷转移通道中参与 I_3^- 到 I^- 的还原反应。本研究展示的结果有望为研究人工光合作用电荷转移过程的机制和构建高效的光电极提供一些启发。

关键词：光敏剂；TiO_2 纳米棒；扫描光电化学显微镜；光激发电子转移